Simulation of ice-ocean dynamics in the Weddell Sea. Part I: Model configuration and validation

R. Timmermann, A. Beckmann, H.H. Hellmer

Alfred Wegener Institute for Polar and Marine Research, Germany

Short title:

Abstract. In the framework of the *Bremerhaven Regional Ice Ocean Simulations* (BRIOS) a coupled sea ice-ocean model, based on a dynamic-thermodynamic sea ice-model and the *S-coordinate Primitive Equation Model* (SPEM) has been developed. The model is run on a circumpolar grid which is focussed on the Weddell Sea. It includes the major Antarctic ice shelves; ice shelf-ocean interaction is described by the sea ice-model's thermodynamic component. Numerical simulations are forced with 6-hourly data of the ECMWF-reanalysis of the period 1985-1993 and validated against observations of hydrography as well as sea ice extent, thickness and drift. Qualitatively and quantitatively, a good agreement with observations is achieved. The basin-wide circulation features a double-cell structure of the Weddell Gyre with maximum transports close to recent observations. Summer sea ice coverage is underestimated but winter ice extent as well as sea ice thickness and drift are well reproduced.

1. Introduction

The importance of the high latitude oceans as water mass transformation regions has motivated numerous studies on ocean circulation, sea ice–ocean interaction and variability of these processes on seasonal and interannual time scales. Most observational and modeling activities are focussed on the Arctic Ocean [see *Aagaard and Carmack*, 1994, for an overview]; much less has been done in the Southern Ocean [*Fahrbach et al.*, 1998]. In both regions, the use of remote sensing data has increased our knowledge considerably.

The ocean circulation in these areas is driven by atmosphere–ocean interaction that is moderated by the occurrence of sea ice. Modeling of this system therefore requires a prognostic sea ice model that captures both the thermodynamic and dynamic processes. In recent years, dynamic–thermodynamic sea ice models have been coupled to oceanic general circulation models in the Arctic [*Häkkinen and Mellor*, 1992; *Zhang et al.*, 1998; *Zhang et al.*, 1999]. In the Southern Ocean, the Weddell Sea has attracted the most attention. However, previous coupled sea ice ocean models in that area [e.g., *Häkkinen*, 1995; *Toggweiler and Samuels*, 1995] had difficulties to cover some of the relevant processes detailed enough to achieve an overall realistic simulation of sea ice coverage and hydrography.

Current efforts made in high latitude modeling aim in two directions:

1. Increasing the resolution of regional models to get a more and more realistic representation of coastline, topography, and oceanic variability [e.g., *Zhang and Semtner*, 1998]. In parallel, improvements of the sea ice component by adding more physical processes are underway [e.g., *Haapala*, 2000].

2. Using coarse resolution global climate models that allow long-term integrations [e.g., *Kim and Stössel*, 1998; *Goosse and Fichefet*, 1999]. Here, model evaluation is often restricted to the identification of physical and numerical sensitivities and plausbility checks of integrated values. In a regional circumpolar model, *Marsland and Wolff* [1999] achieved a quite realistic simulation but their horizontal grid is focussed on the Australian sector of the Southern Ocean and thus processes in the Weddell Sea were not specifically considered.

Our concept follows a third path: We use a relatively coarse resolution which is suitable for climate models and allows integrations over several decades but is fine enough to cover regional processes as far as they appear important for the coupled system's behaviour. Wherever data are available, we perform a quantiative validation.

In a previous study [*Beckmann et al.*, 1999], a stand-alone ocean model has been developed which was able to represent many aspects of the Weddell Sea *time-mean* circulation and water mass distribution quite reliably. The model, forced with climatological data from a sea ice-mixed layer model, served also as a tool for testing subgridscale parameterizations. The logical next step, a fully coupled ice–ocean model, is presented in this paper. Chapter 2 describes the coupled model, with emphasis on coupling strategy. In Chapter 3, the model is validated against observations of sea ice concentration, thickness, drift, as well as large scale transport and water mass distribution in the Weddell Sea. Chapter 4 summarizes our findings. In part II of this study [this issue], the model will be used to investigate the effects of interannual atmospheric variability on sea ice production, sub-ice shelf interaction and water mass formation in the Weddell Sea.

2. The Coupled Model

The coupled ice-ocean model developed for this study is called BRIOS-2 and is based on a hydrostatic regional ocean circulation model and a dynamic-thermodynamic sea ice-model which is also applied to ice shelf-ocean interaction.

2.1. Ocean Model

The ocean component of BRIOS-2 is based on the S-coordinate Primitive Equation Model SPEM [*Haidvogel et al.*, 1991] which has been configured for the Antarctic circumpolar ocean. In a standalone version, it has been used to study the large-scale circulation and water mass distribution in the Weddell Sea [*Beckmann et al.*, 1999]. Subgrid-scale parameterizations presented in that publication for the standalone ocean model have been adopted for the coupled model BRIOS-2. Adaptive mixing schemes were found to be essential in keeping the simulated hydrography close to observations: The *Pacanowski and Philander* [1981] mixing scheme ensures that vertical mixing is continuously increased for a weakening stratification. To avoid unrealistic deep convection in the central Weddell Sea, it turned out to be crucial to have the vertical diffusivity limited by a maximum value of 10^{-2} m^2 s^{-1}. Horizontal diffusivity depends on the local Reynolds number to account for along-flow mixing while cross-flow diffusion is strongly reduced. An additional, grid-spacing dependent background diffusity in the surface and the bottom layer represents the effect of wind-induced near-surface mixing and increased turbulence in the bottom boundary layer.

2.2. Ice Model

The ice component of BRIOS-2 is a dynamic-thermodynamic sea ice model with a viscous-plastic rheology [*Hibler*, 1979] and the *Parkinson and Washington* [1979] thermodynamics using the *Semtner* [1976] zero-layer approach for heat conduction. The model includes a prognostic snow layer [*Owens und Lemke*, 1990] accounting for the effect of flooding [*Leppäranta*, 1983; *Fischer*, 1995]. Model parameters (ice strength parameter $P^* = 20000$ N m^{-2}, lead closing parameter $h_0 = 1.0$ m, others see below) have been chosen following previous studies with a stand-alone version of the sea ice model [*Kreyscher*, 1998; *Harder and Fischer*, 1999]

While application of this sea ice model to the Weddell Sea is somewhat traditional, in this study the model is also used to compute the ice-ocean interaction at the ice shelf base. At ice shelf grid points, ice concentration A is set to 100%; ice thickness h_i is prescribed to be constant in time; ice drift velocity $\vec{u}_i$ is set to zero. Thus, the sea ice model is reduced to its thermodynamic component. In the entire model domain, freezing temperature is computed as a function of hydrostatic pressure and salinity. While this does not significantly affect sea ice-ocean interaction, it is essential for a model to be applied to sub-ice shelf processes. *Hellmer and Olbers* [1989] introduced a model of ice shelf-ocean interaction which determines the *in situ*-freezing point from a diagnostic salinity balance at the ice-ocean interface. In contrast to that, we compute the freezing point as a function of salinity in the uppermost ocean model layer.

2.3. Ice-Ocean Coupling

Ice and ocean model communicate by the exchange of heat, fresh water (salt) and momentum.

Heat Flux. Following *Morison et al.* [1987], the heat flux between ocean and the sea ice base is parameterized as

$$Q_{oi} = \rho_w c_{p,w} c_{h,io} u_* (T_o - T_f), \tag{1}$$

where ρ_w and $c_{p,w}$ denote density and specific heat capacity of sea water at constant pressure, respectively. The transfer coefficient is $c_{h,io} = 1.2 \cdot 10^{-2}$. Friction velocity u_* is calculated as

$$u_* = \sqrt{c_{d,io}}\,|\vec{u}_w - \vec{u}_i| \tag{2}$$

where $\vec{u}_w$ and $\vec{u}_i$ denote the velocity in the uppermost layer of the ocean model and the sea ice velocity, respectively, and $c_{d,io} = 3 \cdot 10^{-3}$ is the oceanic drag coefficient. The ocean temperature T_o is taken from the uppermost model grid box while the *in situ*-freezing temperature T_f is calculated as a function of

salinity S_o and hydrostatic pressure P_o using the nonlinear equation of *UNESCO* [1978].

While near surface ocean velocities outside the sub-ice shelf cavities are stronlgy determined by the ocean surface stress, friction at the ice shelf base merely is a sink of momentum. Thus, tidal currents become particularly important inside the cavities, but, due to the *rigid lid*-approximation employed in SPEM, they are not covered by our model. Model experiments of *Robertson et al.* [1998] feature maximum velocities around 20 cm s^{-1} in the Filchner-Ronne cavity. To avoid underestimation of heat and fresh water exchange between ocean and ice shelf we abstained from a velocity dependent parameterization of ocean-to-ice shelf heat fluxes and use

$$Q_{oi} = \rho_w c_{p,w} \gamma_T (T_o - T_f) \tag{3}$$

with $\gamma_T = 10^{-4}$ m s^{-1} [*Hellmer und Olbers*, 1989] instead. This is equivalent to the velocity dependent approach (1, 2) with a relative velocity of $|\vec{u}_w - \vec{u}_i| = 0.15$ m s^{-1}.

In the open water part of each grid cell, the surface heat flux Q_{ow} is computed using the balance of *Parkinson and Washington* [1979] with dedicated albedo values to account for the different surface properties. In case the ocean has been cooled down to its surface freezing temperature, additional heat loss is converted into sea ice formation.

The total ocean surface heat flux Q_o is computed as a weighted average

$$Q_o = (1 - A) \cdot Q_{ow} - A \cdot Q_{oi} \tag{4}$$

of these contributions.

Transmission of Solar Radiation. In model regions with a high vertical resolution, the incoming solar radiation is not fully absorbed within the ocean model's uppermost layer. Intensity in a depth z below the surface is described as an exponential profile:

$$Q_{SW}(z) = (1 - A) \cdot (1 - \alpha_{ow}) \cdot Q_{SW}^{\downarrow} \cdot e^{-\lambda z}, \tag{5}$$

where $Q_{SW}^{\downarrow}$ denotes the incoming solar radiation (calculated as part of the sea ice model), $\alpha_{ow} = 0.1$ is the open water albedo, and $\lambda = 0.04$ m^{-1} denotes the absorption coefficient. This radiation flux is transmitted vertically and contributes to the heat budget of near-surface grid boxes. Thus, an unrealistic increase of summer sea surface temperature in shallow regions, i.e. in regions with a high vertical resolution is inhibited.

Salt flux. The salt flux related to freezing and melting of ice and snow is computed as

$$\mathcal{F}_i^S = (S_o - S_i) \frac{\rho_i}{\rho_w} \left(\frac{\partial h_i}{\partial t} \right)_{th} + S_o \frac{\rho_{sn}}{\rho_w} \left(\frac{\partial h_{sn}}{\partial t} \right)_{th}, \tag{6}$$

where h_i and h_{sn} are the ice and snow thicknesses, respectively, and the subscript $_{th}$ indicates that only thermodynamic changes of ice and snow volume are considered. Sea ice salinity S_i is assumed to be 5 psu while salinity of snow is assumed to be zero. Salinity of the uppermost ocean model layer is denoted as S_o. Densities of sea ice and snow are $\rho_i = 910$ kg m^{-3} and $\rho_{sn} = 290$ kg m^{-3}, respectively.

Another source of fresh water is the difference between precipitation and evaporation which is denoted as $\mathcal{P} - \mathcal{E}$. As long as the air temperature exceeds the freezing temperature of fresh water ($T_a \geq 0$°C), it is assumed that precipitation falls as rain which completely runs into the ocean. For $T_a < 0$°C, precipitation in the ice covered part of the grid cell is accumulated as snow while precipitation in the open water part still provides a fresh water flux for the ocean model. Thus, the salinity flux in the open ocean part of each grid cell is

$$\mathcal{F}^S_{ow} = S_o \cdot \begin{cases} \mathcal{P} - \mathcal{E} & \text{if} \quad T_a \geq 0°C \\ (1 - A) \cdot (\mathcal{P} - \mathcal{E}) & \text{if} \quad T_a < 0°C \end{cases} \tag{7}$$

and the total salinity flux is

$$\mathcal{F}^S = \mathcal{F}^S_i + \mathcal{F}^S_{ow}. \tag{8}$$

Momentum Flux. Surface stress at the ice-ocean interface is computed using the bulk formula

$$\vec{\tau}_{io} = \rho_w c_{d,io} \left|\vec{u}_i - \vec{u}_w\right| \left((\vec{u}_i - \vec{u}_w) \cos\Theta + \vec{k} \times (\vec{u}_i - \vec{u}_w) \sin\Theta \right) \tag{9}$$

with an turning angle $\Theta = 10°$ which has been chosen after a series of sensitivity experiments described below. The ocean velocity $\vec{u}_w$ is taken from the uppermost ocean model grid point.

In the open water part of each grid cell, the surface stress is parameterized as

$$\vec{\tau}_{ao} = \rho_a c_{d,ao} \left|\vec{u}_{10}\right| \vec{u}_{10} \tag{10}$$

using $c_{d,ao} = 1.0 \cdot 10^{-3}$. Here, we assume that the ocean surface velocity is negligible compared to the 10 m-wind speed $\vec{u}_{10}$. This is consistent with the parameterization of sea ice surface stress where a similar assumption is used to simplify the sea ice momentum balance [*Hibler*, 1979]. The surface stress can be assumed to be parallel to the wind speed $\vec{u}_{10}$ [*Stössel*, 1992]; thus there is no turning angle in this parameterization.

The total ocean surface stress is computed as an area weighted average using

$$\vec{\tau}_o \quad = \quad A \cdot \vec{\tau}_{io} + (1 - A) \cdot \vec{\tau}_{ao} \tag{11}$$

which is consistent with Newton's third law (actio = reactio). As the sea ice model is run on an Arakawa-B grid, while SPEM uses a C grid [*Arakawa and Lamb*, 1977] for horizontal discretization, velocities and stresses are interpolated bilinearly between ice and ocean model.

2.4. Configuration for the Weddell Sea

The coupled model is run on a circumpolar grid which comprises the whole ocean south of 50°S. It focusses on the Weddell Sea where the grid is isotropic with horizontal resolutions of 1.5° zonally and $1.5° \cos\phi$ meridionally [see *Beckmann et al.*, 1999 or *Timmermann et al.*, 2000]. The model domain includes the major Antarctic ice shelves; in the Weddell Sea these are Larsen Ice Shelf (LIS), Filchner-Ronne Ice Shelf (FRIS) and the Eastern Weddell Ice Shelves (EWIS). As described for the standalone ocean model BRIOS-1 [*Beckmann et al.*, 1999], we use 24 layers with an increasing resolution near the surface and the bottom and applied bottom topography and ice shelf thickness data from *Johnson and Smith* [1997], *Smith and Sandwell* [1997], and *Schenke et al.* [1998].

Initial conditions as well as Θ-S-fields on the northern boundary were derived from the Hydrographic Atlas of the Southern Ocean [*Olbers et al.*, 1992]. A barotropic transport of 130 Sv through Drake Passage is prescribed. Half of this ACC transport is prescribed to leave the model domain east of Drake Passage and is gradually refed in the Indian sector of the Southern Ocean.

The model is forced with 6-hourly data of 10-m wind, total cloudiness, and 2-m air and dew point temperature from the ECMWF reanalyses of 1985-1993. As the ECMWF $\mathcal{P} - \mathcal{E}$ dataset was not available for this study, daily precipitation and evaporation fields were derived from the NCEP reanalysis. No flux correction is applied.

A time step-splitting technique is used for computational efficiency: The time step is 6 hours for the sea ice model while the high vertical resolution on the continental shelf requires an ocean time step of 11.25 min (128 time steps per day). To reduce generation and transmission of inertial oscillations, the ocean surface stress is interpolated between two calls of the sea ice model while the ocean surface velocity $\vec{u}_w$ is averaged over the same period.

Two passes of the nine-year period 1985-1993 are used to obtain a quasi-stationary seasonal cycle of surface temperature and sea ice distribution. Results presented in this paper are from the third 9-years integration.

3. Model results and validation

3.1. Time-mean Circulation and Hydrography

A prominent (and robust) feature of the simulated ocean circulation in the Weddell Sea is a pronounced double-cell structure quite similar to the results obtained with the standalone ocean model

BRIOS-1 [*Beckmann et al.*, 1999] (Fig. 1). Transports across the line Kapp Norvegia – Joinville Island and across the Greenwich meridian compare well with the measurements of *Fahrbach et al.* [1994] and *Schröder and Fahrbach* [1999], respectively. Like in BRIOS-1, the double-cell structure is pronounced only below 500 m depth, while in the near-surface currents the influence of the large scale wind field is dominant. Outside the Weddell Sea, the Kerguelen and Ross gyres appear as closed cyclonic circulations with maximum transports of 31 and 23 Sv, respectively.

Timmermann et al., [2000] show that water mass properties in BRIOS-2 are in good agreement with observations. The seasonal and interannual variability will be discussed in part II of this study [this issue].

3.2. Sea ice extent

Time series of simulated sea ice extent (as defined by the area with ice concentrations > 15 %) indicate that the model reaches a quasistationary seasonal cycle after only one or two years (Fig. 2). Simulated winter sea ice covers an area of about $20 \cdot 10^6\,\mathrm{km}^2$ which is in good agreement with analyses of the PELICON-project [*Heygster et al.*, 1996]. In contrast, simulated summer sea ice extent appears to be underestimated by roughly 40 %.

As the sea ice extent is quite sensitive to advection of heat by ocean currents, even small variations of the temperature and velocity fields may have a significant impact on sea ice distribution in the respective area. In general, sea ice models face the problem that the surface heat budget consists of several large contributions with different signs which add to a residuum that is smaller by one or two orders of magnitude. Even minor errors in one of the contributions may lead to pronounced modifications of the surface heat balance and thus freezing and melting rates. Consequently, both errors in the forcing data and numerical errors may lead to substantial deviations from the observed sea ice distribution. It is therefore even more surprising that in the 27-year coupled simulation only little drift in sea ice or ocean variables exists.

The simulated minimum sea ice distribution (Fig. 3) features a lack of sea ice near the tip of the Antarctic Peninsula and in the Amundsen and Bellingshausen Seas. We attribute the first to a poor representation of the Antarctic Peninsula in the atmospheric forcing fields [see *Timmermann*, 2000] and the latter to the model's coarse resolution in the Pacific sector.

During austral winter, Antarctica is enclosed by a compact sea ice cover (Fig. 4). Each of the three major gyres (Fig. 1) leads to a northward spreading of sea ice, most pronounced in the Weddell

sector. Northward sea ice extent is limited by the position of the Antarctic Circumpolar Current (ACC) which even in winter has surface temperatures above the freezing point and acts as a permanent heat source. In addition, strong westerly winds induce a mainly zonal sea ice drift. As the course of the ACC in the model is largely determined by bottom topography and has been optimized by varying the northern boundary conditions, winter sea ice extent in BRIOS-2 is in remarkably good agreement with observations. In appendix A, we will discuss the sensitivity of these results to the parameterization of vertical mixing.

3.3. Sea ice thickness

Like the winter ice extent, the simulated sea ice thickness distribution during the austral winter maximum (Fig. 5) appears to be thoroughly reasonable: The thickest ice is found in the southwestern Weddell Sea where net freezing rates of up to 4 m yr^{-1} [*Timmermann et al.*, 2000] and deformation of sea ice along the Antarctic coast lead to a typical maximum ice thickness of 3 m. Locally, ice thickness may exceed 5 m, but the locations of maximum thickness vary interannually so that the climatological mean is much smaller than the actual maxima.

In the central Weddell Sea, typical winter sea ice thickness is 1-1.5 m which is only slightly thicker than can be achieved by purely thermodynamic sea ice growth [*Harder und Lemke*, 1994]. Obviously, sea ice deformation does not play a major role in the buildup of sea ice volume here. A strong meridional gradient can be seen only outside the Weddell Sea.

For the validation of sea ice thickness we used measurements of upward looking sonars (ULS) [*Strass and Fahrbach*, 1998] which were deployed on the line Kapp Norvegia - Joinville Island during 1991/1992 and 1993/1994 (Fig. 6).

While the ULS has a footprint of roughly 10 m in diameter, the simulated ice thickness interpolated to the ULS position includes information from an area of roughly 10 000 km^2. To allow for a meaningful comparison, we averaged the observed ice draft over a period of one week.

Time series of simulated and observed ice thickness (Fig. 7) indicate that especially at the offshore mooring positions 217, 208, 209, and 210 the model is in good agreement with observations. The same is true for the easternmost, near-coast position 212, but the observed variability at this ULS is much higher than simulated. Both in nature and in the model, sea ice is deformed in case of onshore winds. However, relevant scales for this process are much smaller than the grid size, so that the variability of the ULS point measurement can hardly be reproduced by the modeled mean thickness. Finally, the

underestimation of ice volume at the westernmost position 207 is attributed to the overestimation of melting in that region (see above) which prevents the survival of multi-year ice.

Due to missing coherence between ULS deployment and modelled years, a quantitative comparison to ULS data along the Greenwich Meridian is not possible. However, the simulated sea ice thickness distribution agrees qualitatively with the meridional profile of *Harms et al.* [2000].

3.4. Sea ice drift

The large scale sea ice drift (Fig. 8) reflects the general patterns of atmospheric and oceanic circulation: The basin-wide cyclonic circulation of the Weddell Gyre is clearly visible. However, akin to the ocean surface currents, a double-cell structure is absent. Minimum drift velocities are found in the southern Weddell Sea where a compact ice cover is subject to strong internal forces. Maximum mean drift velocities of more than 15 cm s^{-1} are found near the northern sea ice edge, where forcing by both the ACC and the strong westerly winds together with the virtual absence of internal friction lead to increased sea ice drift velocities.

To validate sea ice drift fields we use Lagrangian trajectories derived from ARGOS buoys which were deployed in the Weddell Sea in 1986 [*Argos Collect Localisation Satellites Company*, 1988; *Kottmeier und Hartig*, 1990]. A model buoy is released at the start position of each ARGOS buoy. Its trajectory is computed using velocity components interpolated linearly in time and space onto the actual position until the buoy encounters open water. Here, the sea ice momentum balance becomes meaningless and integration is stopped. Additional buoys are released every 60 days along the observed trajectory, thus generating an ensemble of trajectories along the observed track (Fig. 9). Every 30 days, a mark is set on the trajectory. Dispersion of these marks gives a measure of the correspondence between simulated and observed sea ice drift. As *Harder and Fischer* [1999] pointed out, a buoy which has lost track of the observed path is forced by different velocity fields and may well diverge further from the observed trajectory. However, coherence between observed and simulated trajectories in BRIOS-2 is high enough to keep the differences between individual tracks of each bundle quite low.

A series of sensitvity studies was performed to identify critical parameters of the sea ice momentum balance and to optimize the sea ice drift fields in the coupled model. It turned out that the simulated sea ice drift is not only sensitive to the ratio of oceanic and atmospheric drag coefficient [*Fischer and Lemke*, 1994] but also to the turning angle Θ in Eq. (9) which has to be chosen according to the vertical resolution near the ocean surface. In BRIOS-2, the best agreement between modeled and observed

trajectories is achieved using $\Theta = 10^{\circ}$ (Fig. 9), which is consistent with the fact that BRIOS-2's uppermost ocean grid point is located within the Ekman layer. Varying the atmospheric and oceanic drag coefficients from their standard values of $c_{d,ai} = 1.32 \cdot 10^{-3}$ and $c_{d,io} = 3 \cdot 10^{-3}$ [*Fischer*, 1995] does not lead to further improvement of simulated sea ice drift.

Obviously, a realistic description of momentum exchange between sea ice and ocean is essential to achieve a realistic sea ice drift. Trajectories from a series of simulations with different values for Θ (not shown) reveal quite similar short scale deviations from the mean trajectory which are caused by passing cyclones. Thus, synoptic variability of near-surface winds is reflected by quasi-stochastic ice drift patterns. The large scale drift, however, is largely determined by sea ice-ocean momentum exchange. The ocean is not simply a sink for the sea ice momentum balance; near surface currents dominate the large-scale, basin-wide sea ice drift. The coherence of simulated and observed sea ice drift in BRIOS-2 is significantly improved compared to the simulations of *Harder and Fischer* [1999] who used a very similar sea ice-model, but with fixed ocean currents from *Olbers and Wübber* [1991], and underestimated the mean sea ice drift speed significantly (especially in the northern part of the Weddell Sea). We conclude that an adequate sea ice-ocean momentum coupling is crucial to achieve realistic basin-scale sea ice drift patterns.

4. Conclusions

We presented a newly developed coupled ice-ocean model for the Weddell sector of the Southern Ocean which describes ice shelf-ocean interaction by a subset of the sea ice model equations. Validation with respect to large scale ocean circulation, and sea ice extent, thickness and drift revealed - even locally - a good agreement with observations. Compared to earlier studies in this region, the use of high frequency forcing data and of a relatively high vertical resolution in shallow regions due to the ocean model's s-coordinate contribute to a close-to-reality description of the coupled ice-ocean system. The *Pacanowski and Philander* [1981] mixing scheme has been shown to be suitable not only for standalone high latitude ocean models [Beckmann et al., 1999] but also for coupled ice-ocean modeling. The transmission of solar radiation through the uppermost ocean layers prevents the ocean surface from unrealistic temperature increases during the austral summer. An appropriate choice of the turning angle in the ice-ocean stress parameterization turned out to be crucial for a good reproduction of the observed sea ice drift. Remaining deficiencies in summer sea ice cover can be attributed to a poor representation of the atmospheric flow close to the Antarctic Peninsula in the forcing data, and to the

coarse resolution outside the Weddell Sea sector.

Though not eddy-resolving, the overall good agreement with observations indicates that the model is able to reproduce regional features of the ice-ocean interaction. The time step splitting scheme ensures efficient use of computer resources. The absence of a significant trend in the sea ice coverage allows long-term integrations as well as investigations of interannual variability. Part II of this study [this issue] will address this subject.

Appendix A: Sensitivity to parameterization of vertical mixing

During development and optimization of the coupled model, we performed a series of sensitivity studies with respect to parameterizations of horizontal and vertical mixing. It turned out that an adequate parameterization of convection is crucial for a realistic reproduction of both observed hydrography and sea ice properties.

Using the traditional convective adjustment scheme [*Rahmstorf*, 1993] leads to the formation of a large polynya in the central Weddell Sea (Fig. 10) and to a rapid homogenization of the water column down to 3000 m depth (Fig. 11 a). Variations of sea ice or coupling parameters within reasonable limits did not solve this problem, and/or caused undesired effects in other model variables. Quite similar results were obtained using an implicit vertical diffusion scheme with a vertical diffusivity of 1 $m^2\ s^{-1}$ in case of static instability. In both cases, quasi-instantaneous mixing led to very large upward heat fluxes which in the simulation caused rapid melting of sea ice. For each convection cell, a vertical diffusivity of the order of 1 $m^2\ s^{-1}$ may be a reasonable approach, but these cells are typically 0.5 to 1 km in diameter [*Schott und Leaman*, 1991; *Send und Käse*, 1998] and thus much smaller than model grid cells in large-scale simulations. Between the individual cells, stratification of the water column is preserved for a while so that effective, grid-cell scale mixing is considerably smaller.

Model results were greatly improved by reducing the vertical diffusivity for the treatment of static instability to 0.01 $m^2\ s^{-1}$. Evidence of unrealistic convection was significantly reduced. However, this scheme still does not include any representation of near surface wind mixing. Thus, summer mixed layers in these simulations are very shallow (Fig. 11 b) and the refreshing of the near surface water column during sea ice melt is restricted to the uppermost layer.

Finally, we identified the *Pacanowski and Philander* [1981] mixing scheme with 0.01 $m^2\ s^{-1}$ as an upper limit for vertical diffusivity as a suitable parameterization of vertical mixing even in case of convection. Using the Richardson number as a measure of mixing activity, the scheme provides

increased vertical mixing both in case of a strong wind stress (corresponding to an increased vertical shear) and of weak stratification. This scheme introduces a smooth transition between low and high turbulence situations and enables a reasonable reproduction of both sea ice coverage and hydrography (Fig. 11 c).

Acknowledgements

The authors would like to thank W. Cohrs and C. Lichey for preparing the ECMWF and NCEP atmospheric forcing fields received via the German Weather Service (Deutscher Wetterdienst, DWD) and the NOAA-CIRES Climate Diagnostics Center, Boulder, using the website http://www.cdc.noaa.gov/, respectively. Helpful discussions with G. Birnbaum and S. Harms are gratefully acknowledged.

References

Aagaard, K., and E. C. Carmack: The Arctic Ocean and climate: A perspective. In: *The Polar Oceans and Their Role in Shaping the Global Environment, Geophysical Monograph* **85**, 5-20, AGU, Washington, USA, 1994.

Arakawa, A. , and V. R. Lamb: Computational design of the basic dynamical processes of the UCLA general circulation model. *Methods of computational physics*, **17**, 174-265. Academic Press, 1977.

Argos Collect Localisation Satellites Company: User Manual, Toulouse, France, 1988.

Beckmann, A., H. H. Hellmer, and R. Timmermann: A numerical model of the Weddell Sea: large scale circulation and water mass distribution. *J. Geophys. Res.*, **104(C10)**, 23375-23391, 1999.

Fahrbach, E., G. Rohardt, M. Schröder, and V. Strass: Transport and structure of the Weddell Gyre. *Annales Geophysicae*, **12**, 840-855, 1994.

Fahrbach, E., M. Schröder, and A. Klepikov: Circulation and water masses in the Weddell Sea. In: *Physics of Ice-Covered Seas*, **2**, 569-603, University of Helsinki, Finland, 1998.

Fischer, H., and P. Lemke: On the required accuracy of atmospheric forcing fields for driving dynamic-thermodynamic sea ice models. In: *The Polar Oceans and Their Role in Shaping the Global Environment, Geophysical Monograph* **85**, 373-381, AGU, Washington, USA, 1994.

Fischer, H.: Vergleichende Untersuchungen eines optimierten dynamisch-thermodynamischen Meereismodells mit Beobachtungen im Weddellmeer. *Berichte zur Polarforschung* **166**, Alfred-Wegener-Institut (AWI), Bremerhaven, 1995.

Goosse, H., and T. Fichefet: Importance of ice-ocean interactions for the global ocean circulation: A model study. *J. Geophys. Res.*, (in press), 1999.

Haapala, J.: On the modelling of the ice thickness redistribution. *Journal of Glaciology*, **46** (in press).

Haidvogel, D.B., J. L. Wilkin, and R. E. Young: A semi-spectral primitive equation ocean circulation model using vertical sigma and orthogonal curvilinear horizontal coordinates. *J. Comput. Phys.*, **94**, 151-185, 1991.

Häkkinen, S., and G.L. Mellor: Modeling the seasonal variability of a coupled Arctic Ice-Ocean System. *J. Geophys. Res.*, **97(C12)**, 20285-20304,1992.

Häkkinen, S.: Seasonal simulation of the Southern Ocean coupled ice-ocean system. *J. Geophys. Res.*, **100(C11)**, 22733-22748, 1995

Harder, M., and P. Lemke: Modelling the extent of sea ice ridging in the Weddell Sea. In: *The Polar Oceans and Their Role in Shaping the Global Environment, Geophysical Monograph* **85**, 187-197, AGU, Washington, USA, 1994.

Harder, M., and H. Fischer: Sea ice dynamics in the Weddell Sea simulated with an optimized model. *J. Geophys. Res.*, **104(C5)**, 11151-11162, 1999.

Harms, S., E. Fahrbach , and V. H. Strass: Ice transport in the Wedell Sea. *J. Geophys. Res.*, (submitted), 2000.

Hellmer, H. H., and D. Olbers: A two-dimensional model for the thermohaline circulation under an ice shelf. *Antarctic Science*, **1**, 325-336, 1989.

Heygster, G., L. T. Pedersen, J. Turner, C. Thomas, T. Hunewinkel, H. Schottmüller, and T. Viehoff: PELICON: Project for estimation of long-term variability of ice concentration. *EC Contract Report* EV5V-CT93-0268 (DG 12), Bremen, 1996.

Hibler, W. D., III: A dynamic thermodynamic sea ice model. *J. Phys. Oceanogr.*, **9(4)**, 815-846, 1979.

Johnson, M. R., and A. M. Smith: Seabed topography under the southern and western Ronne Ice Shelf, derived from seismic surveys. *Antarctic Science*, **9**, 201-208, 1997.

Kim, Seong-Joong, and A. Stössel: On the representation of the Southern Ocean water masses in an ocean climate model. *J. Geophys. Res.*, **103(C11)**, 24891-24906, 1998.

Kottmeier, Ch., and R. Hartig: Winter observations of the atmosphere over Antarctic sea ice. *J. Geophys. Res.*, **95(D10)**, 16551-16560, 1990.

Kreyscher, Martin: Dynamik des arktischen Meereises - Validierung verschiedener Rheologieansätze für die Anwendung in Klimamodellen. *Berichte zur Polarforschung* **291**, Alfred-Wegener-Institut (AWI), Bremerhaven, 1998.

Leppäranta, M.: A growth model for black ice, snow ice, and snow thickness in subarctic basins. *Nordic Hydrology*, **14**, 59-70, 1983.

Marsland, S. J., and J.-O. Wolff: On the sensitivity of Southern Ocean sea ice to the surface fresh water flux: A model study. *J. Geophys. Res.*, submitted, 1999.

Morison, J. H., M. G. McPhee , and G. A. Maykut: Boundary layer, upper ocean and ice observations in the Greenland Sea marginal ice zone. *J. Geophys. Res.*, **92(C7)**, 6987-7011, 1987.

Olbers, D., and C. Wübber: The role of wind and buoyancy forcing of the Antarctic Circumpolar Current. *Strategies for Future Climate Research*, edited by M. Latif, 161-192, Max-Planck-Institut für Meteorologie, Hamburg, 1991.

Olbers, D., V. Gouretski, G. Seiss, and J. Schröter: Hydrographic atlas of the Southern Ocean. Alfred-Wegener-Institut für Polar- und Meeresforschung, Bremerhaven, 1992.

Owens, W. B., and P. Lemke: Sensitivity studies with a sea ice-mixed layer-pycnocline model in the Weddell Sea. *J. Geophys. Res.*, **95(C6)**, 9527-9538, 1990.

Pacanowski, R. C., and S. G. H. Philander: Parameterization of vertical mixing in numerical models of the tropical oceans. *J. Phys. Oceanogr.*, **11**, 1443-1451, 1981.

Parkinson, C. L., and W. M. Washington: A large-scale numerical model of sea ice. *J. Geophys. Res.*, **84(C1)**, 311-337, 1979.

Rahmstorf, S.: A fast and complete convection scheme for ocean models. *Ocean Modelling* **101**, 9-11, 1993.

Robertson, R., L. Padman, and G. D. Egbert: Tides in the Weddell Sea. In: *Ocean, Ice and Atmosphere: Interactions at the Continental Margin, Antarct. Res. Ser.*, **75**, edited by S.S. Jacobs , and R.F. Weiss, 341-369, AGU, Washington, D. C., 1998.

Schenke, H.W., H. Hinze, S. Dijkstra, B. Hoppmann, F. Niederjasper, and T. Schöne: The new bathymetric charts of the Weddell Sea: AWI BCWS. In: *Ocean, Ice and Atmosphere: Interactions at the Antarctic Continental Margin. Antarctic Research Series*, **75**, edited by S. S. Jacobs and R. F. Weiss, 373-382, AGU, Washington D.C., 1998.

Schott, F., and K. D. Leaman: Observations with moored acoustic Doppler current profilers in the convection regime in the Gulf of Lions. *J. Phys. Oceanogr.*, **21**, 556-572, 1991.

Schröder, M., and E. Fahrbach: On the structure and the transport of the eastern Weddell Gyre, *Deep Sea Res.*, **46**, 501-527, 1999.

Semtner, A. J., Jr.: A model for the thermodynamic growth of sea ice in numerical investigations of climate. *J. Phys. Oceanogr.*, **6(3)**, 379-389, 1976.

Send, U., and R. H. Käse: Parameterization of processes in deep convection regimes. In: *Ocean Modeling and Parameterization*, edited by E. P. Chassignet, and J. Verron, NATO Science Series, **516**, 191-214, 1998.

Smith, W.H.F., and D.T. Sandwell: Global sea floor topography from satellite altimetry and ship depth soundings. *Science*, **277**, 1956-1962, 1997.

Stössel, A.: Sensitivity of Southern Ocean sea ice simulations to different atmospheric forcing algorithms. *Tellus*, **44A**, 395-413, 1992.

Strass, V. H., and E. Fahrbach: Temporal and regional variation of sea ice draft and coverage in the Weddell Sea obtained from Upward Looking Sonars. In: *Antarctic Sea Ice: Physical Processes, Interactions and Variability, Antarctic Res. Ser.*, **74**, edited by M. O. Jeffries, 123-139, 1998.

Timmermann, R.: Wechselwirkungen zwischen Eis und Ozean im Weddellmeer. PhD-thesis, University of Bremen, Germany, electronic publication http://elib.suub.uni-bremen.de/dissertations/physic/Timmermann_R2000/index.html, 130 pp., 2000.

Timmermann, R., A. Beckmann und H. H. Hellmer: The role of sea ice in the fresh water budget of the Weddell Sea. Annals of Glaciology, Vol. 33 (in press), 2000.

Toggweiler, J. R. , and B. Samuels: Effect of Sea Ice on the Salinity of Antartic bottom waters. *J. Phys. Oceanogr.*, **25**, 1980-1997, 1995.

UNESCO: Eighth report of the joint panel on oceanographic tables and standards. *UNESCO Technical Papers in Marine Science*, **28**, UNESCO, Paris, 1978.

Zhang, J., W. Hibler, M. Steele, and O. Rothrock: Arctic ice-ocean modeling with and without climate restoring. *J. Phys. Oceanogr.*, **28**, 191-217, 1998.

Zhang, Y., and A.J. Semtner: Ocean-ice interaction within the Weddell and Cosmonaut Seas from high resolution models. *Ann. Geophys.*, 16 suppl. II, 592, 1998.

Zhang, Y., W. Maslowski, and A.J. Semtner: Impact of mesoscale ocean currents on sea ice in high-resolution Arctic ice and ocean simulations. *J. Geophys. Res.*, **104(C8)**, 18409-18429, 1999.

Received _____

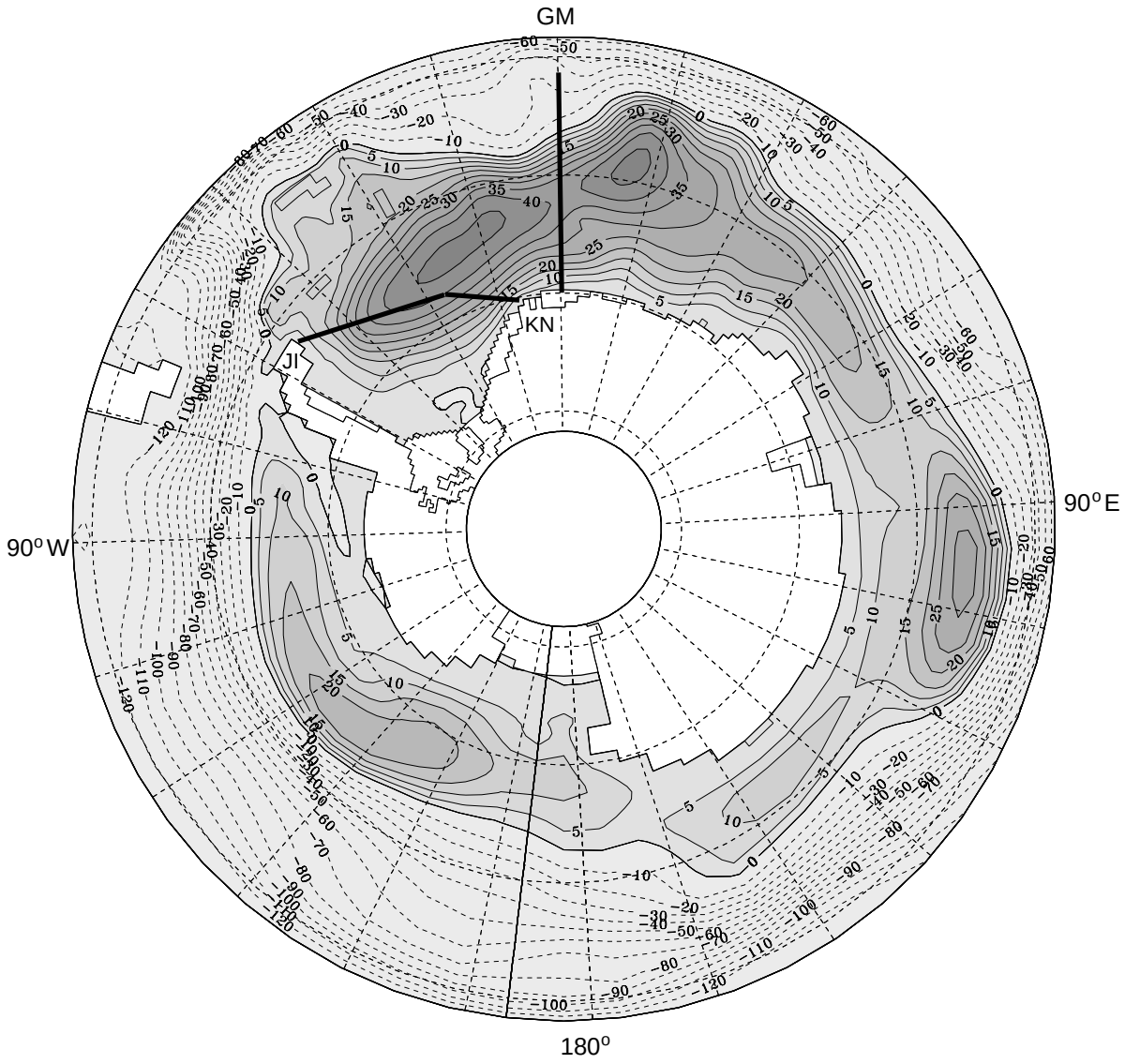

Figure 1. Vertically integrated transport (9-year mean) in the coupled ice-ocean model BRIOS-2. Intervals are 5 Sv for positive (solid) and 10 Sv for negative (dashed) contour lines. Thick solid lines mark the approximate locations of hydrographic sections from which transport estimates were derived by *Fahrbach et al.* [1994] and *Schröder and Fahrbach* [1999]. GM = Greenwich Meridian, JI = Joinville Island, KN = Kapp Norvegia.

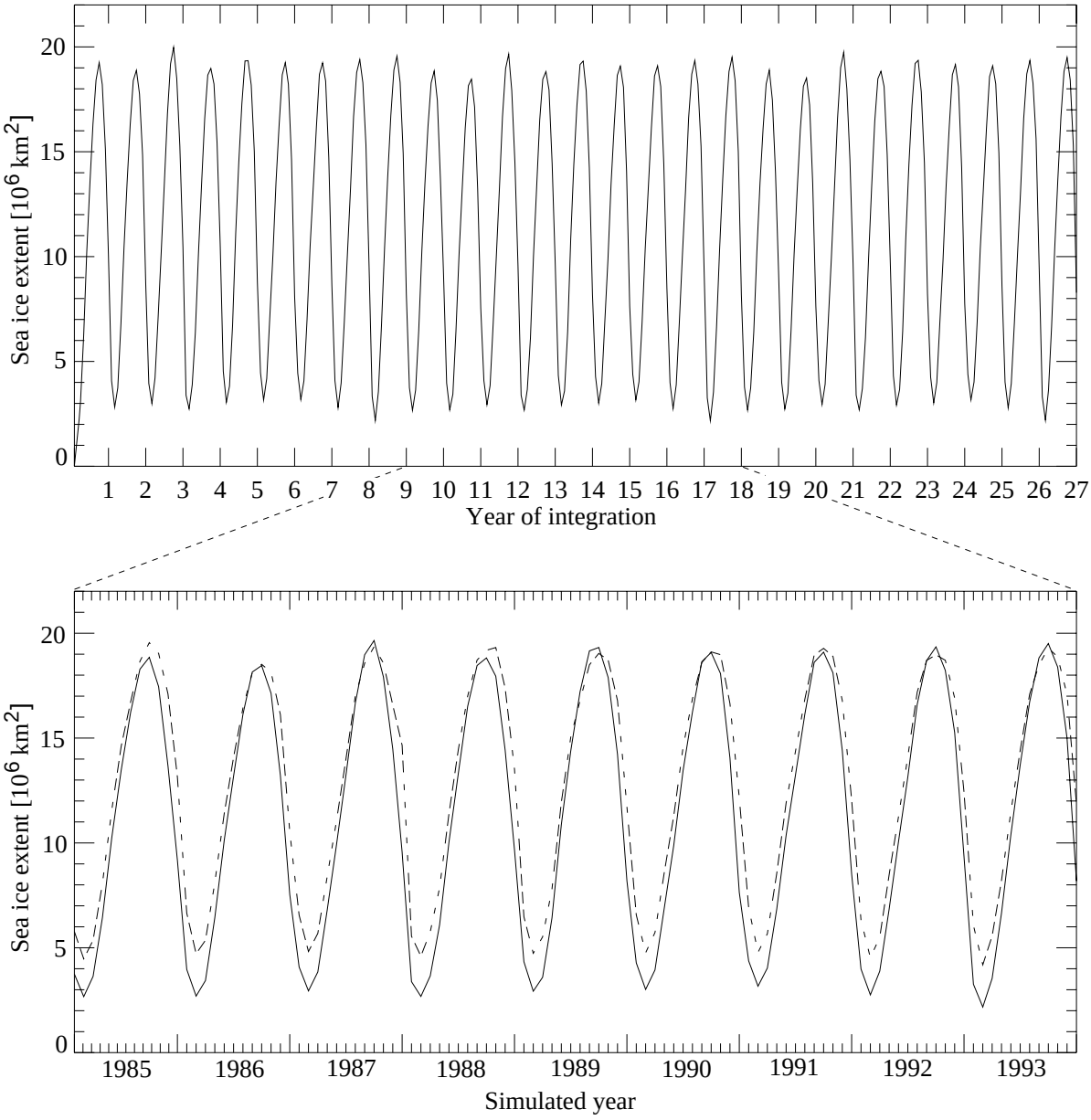

Figure 2. Time series of sea ice extent in the BRIOS-2 reference simulation (top) and comparison with observations from 1985-1993 (bottom). Observed ice extent (dashed) was derived from PELICON data [*Heygster et al.*, 1996].

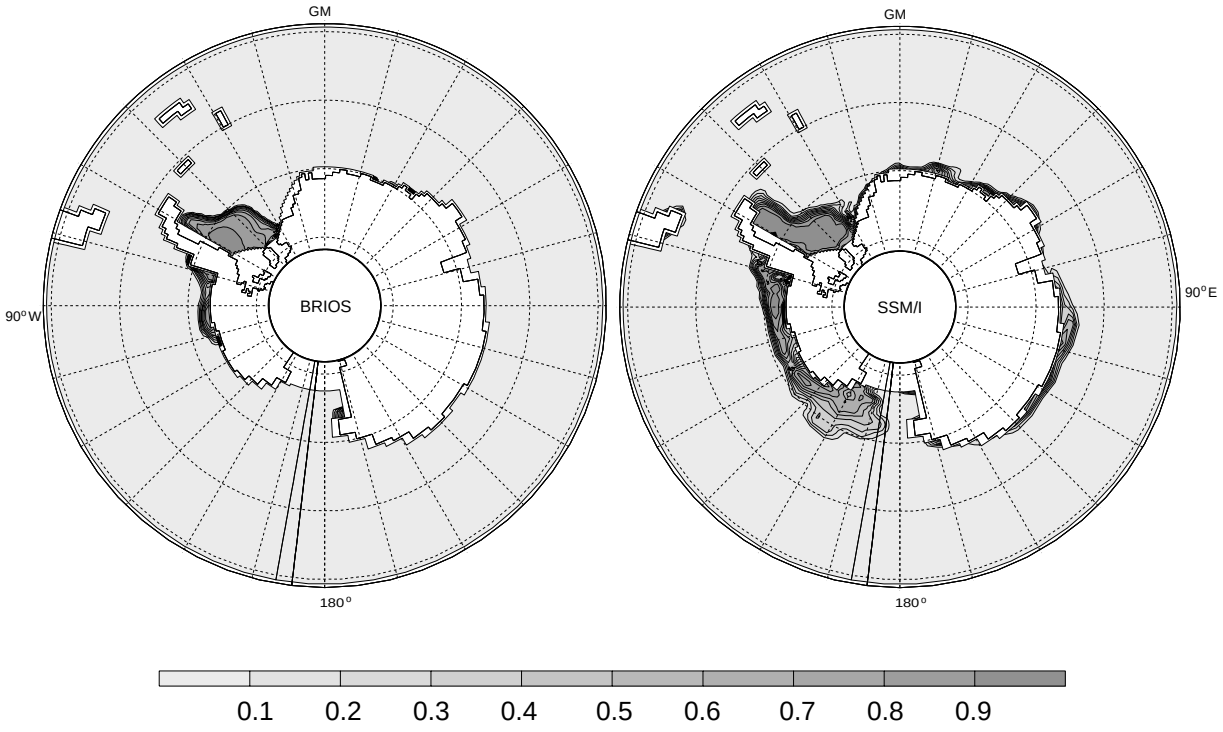

Figure 3. Monthly mean simulated (left) and observed (right) sea ice concentration for Feb. 1987.

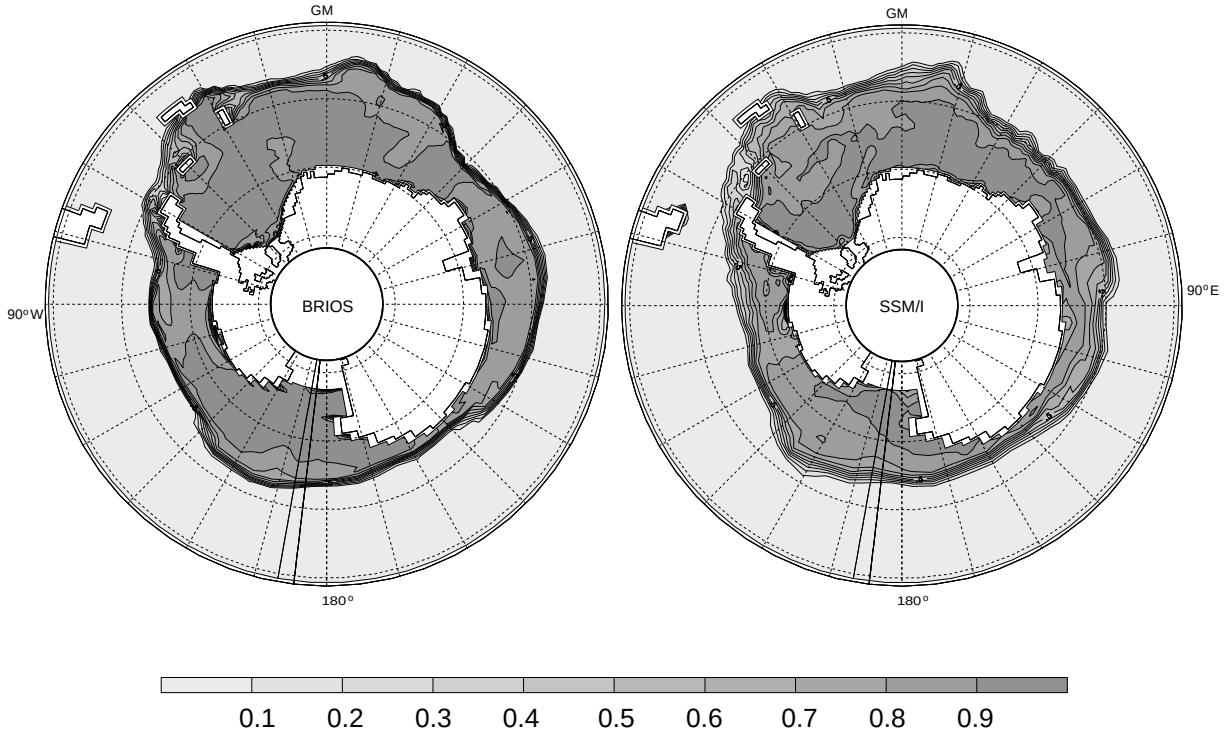

Figure 4. Monthly mean simulated (left) and observed (right) sea ice concentration for September 1987.

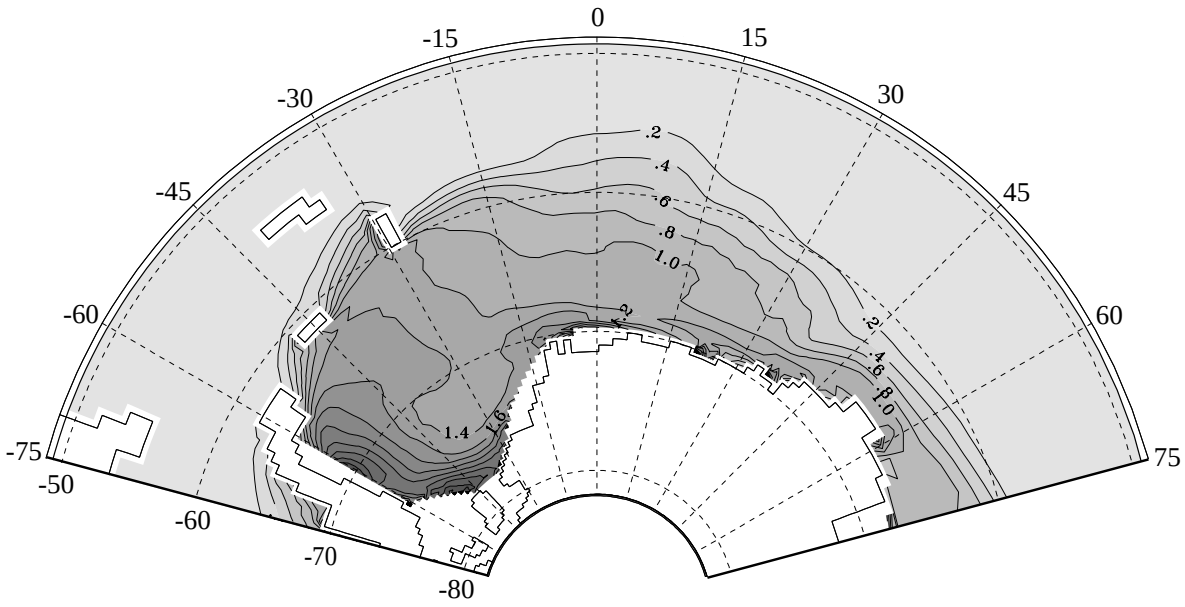

Figure 5. Climatological September mean of the simulated distribution of sea ice thickness [m] in the Weddel sector of the Southern Ocean. Contour interval is 0.2 m.

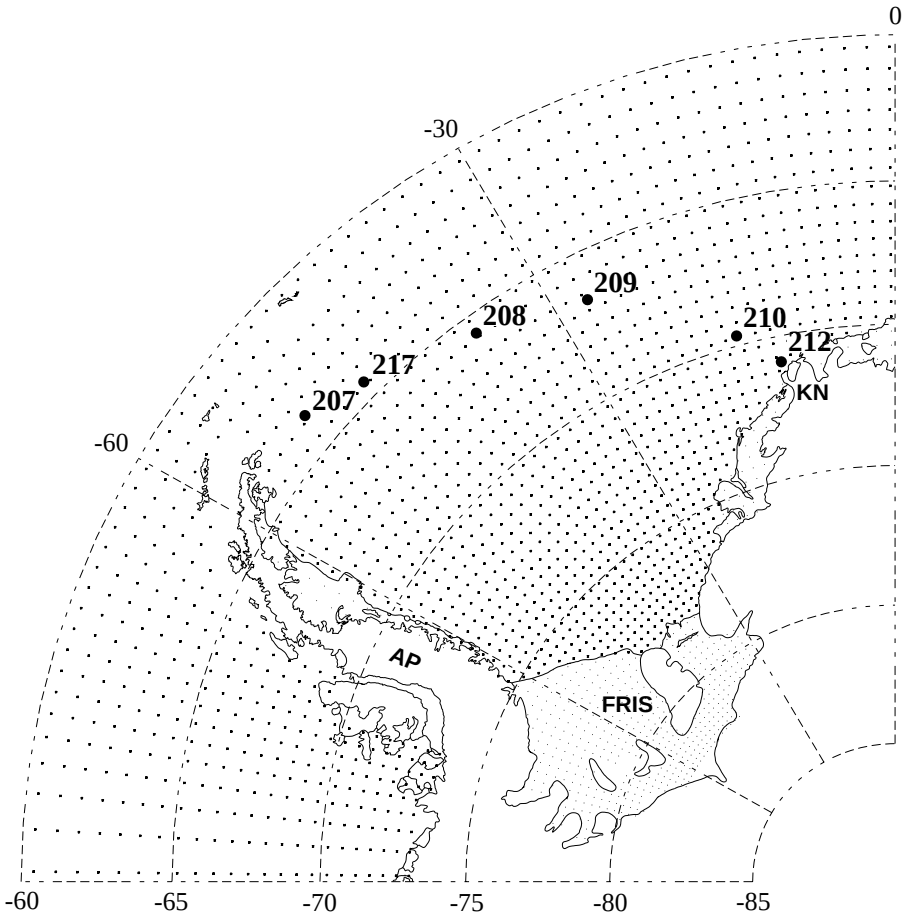

Figure 6. Positions of upward looking sonars (ULS) in the Weddell sector of the BRIOS-2 model grid, indicated by bold dots and the AWI mooring number. AP = Antarctic Peninsula, KN = Kapp Norvegia, FRIS = Filchner-Ronne Ice Shelf.

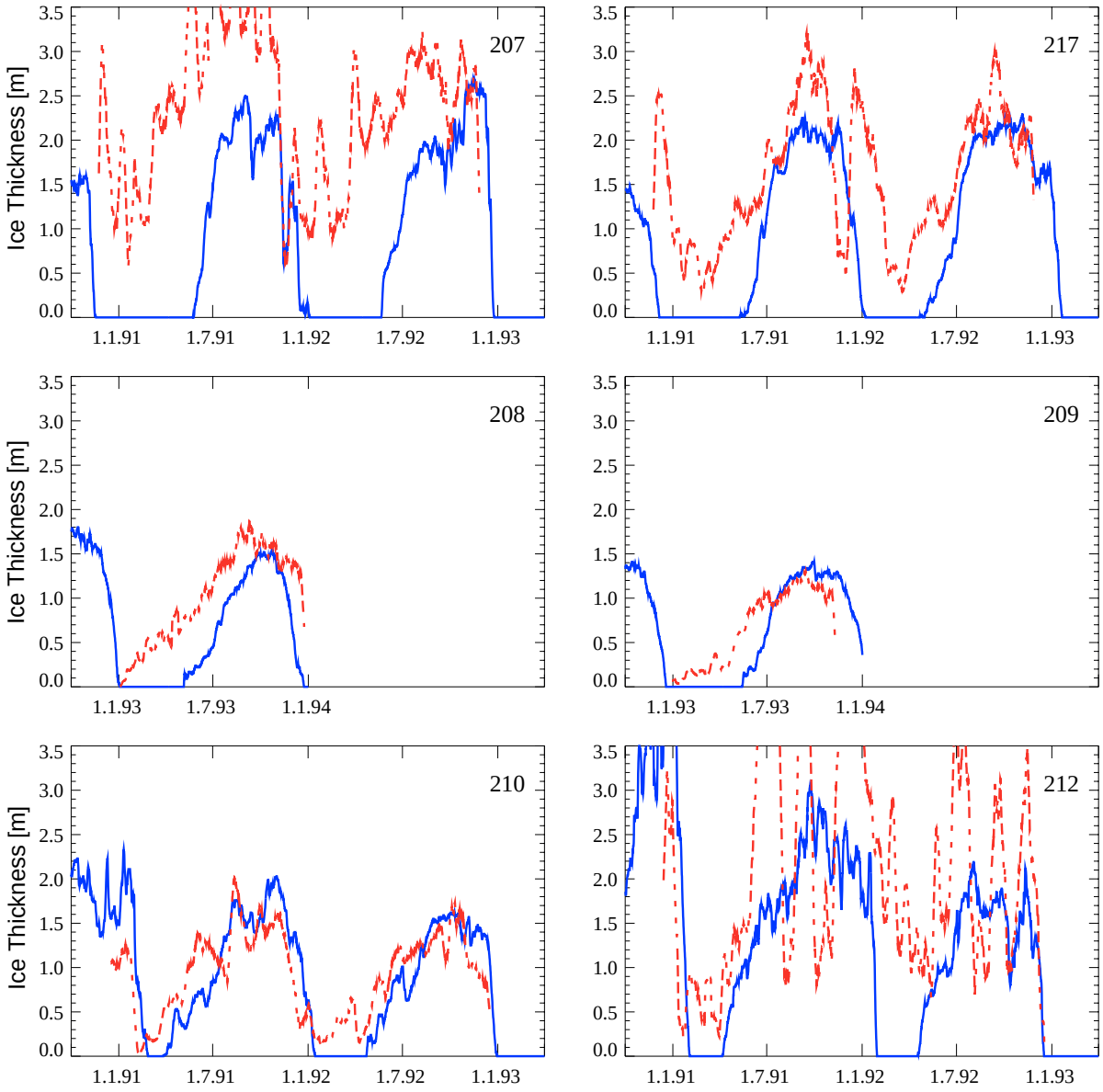

Figure 7. Time series of simulated (solid) and observed (dashed) ice thickness at six ULS positions in the Weddell Sea. Observed thicknesses are weekly means. Positions from west to east.

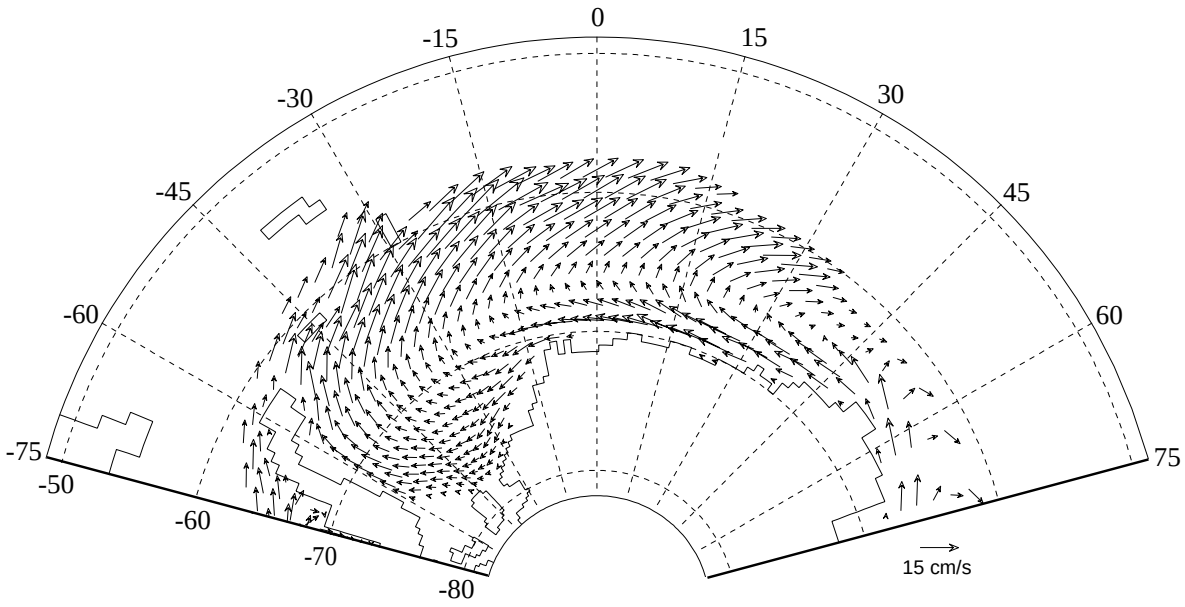

Figure 8. Climatological (1985-1993) September-mean of the simulated sea ice drift in the Weddell sector of the Southern Ocean.

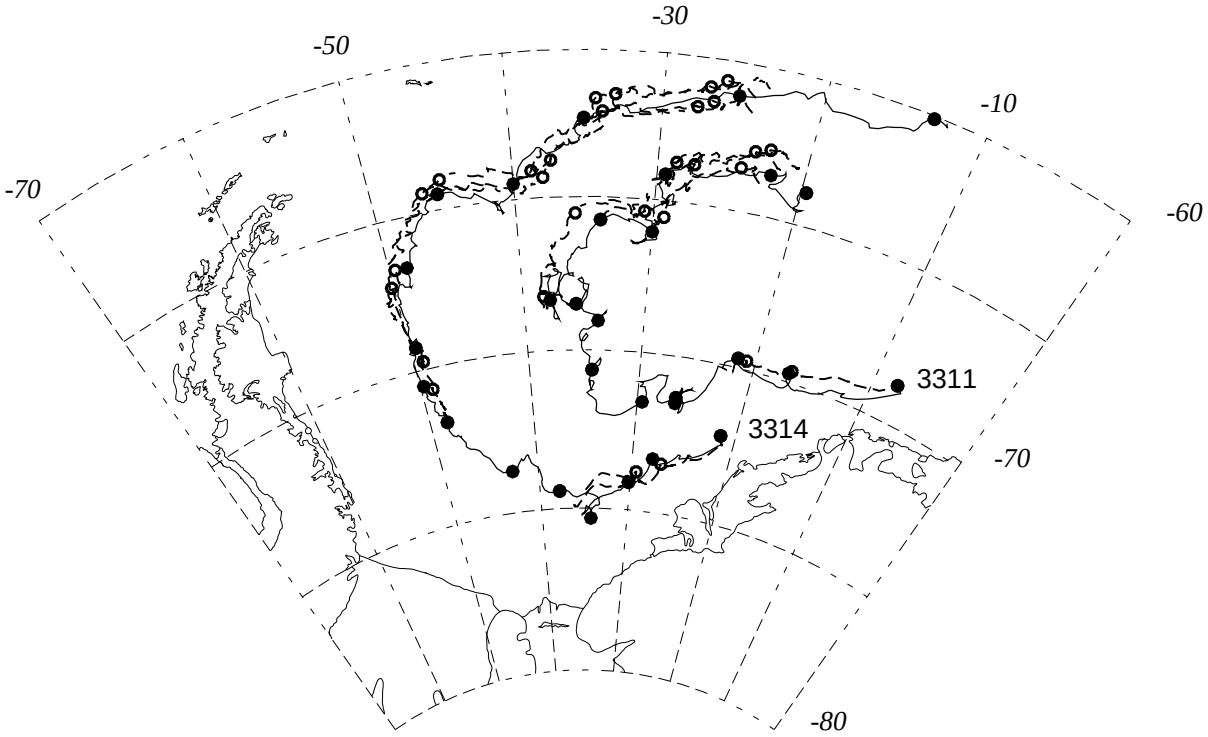

Figure 9. Observed (solid) and simulated (dotted) sea ice drift trajectories from the BRIOS-2 reference experiment. Bold marks are set every 30 days; solid circles refer to observed buoy positions, open circles to the simulated trajectories. Every 60 days a new model buoy is released. Trajectories of the buoys 3311 und 3314 which are displayed here are representative of all five ARGOS buoys used for validation.

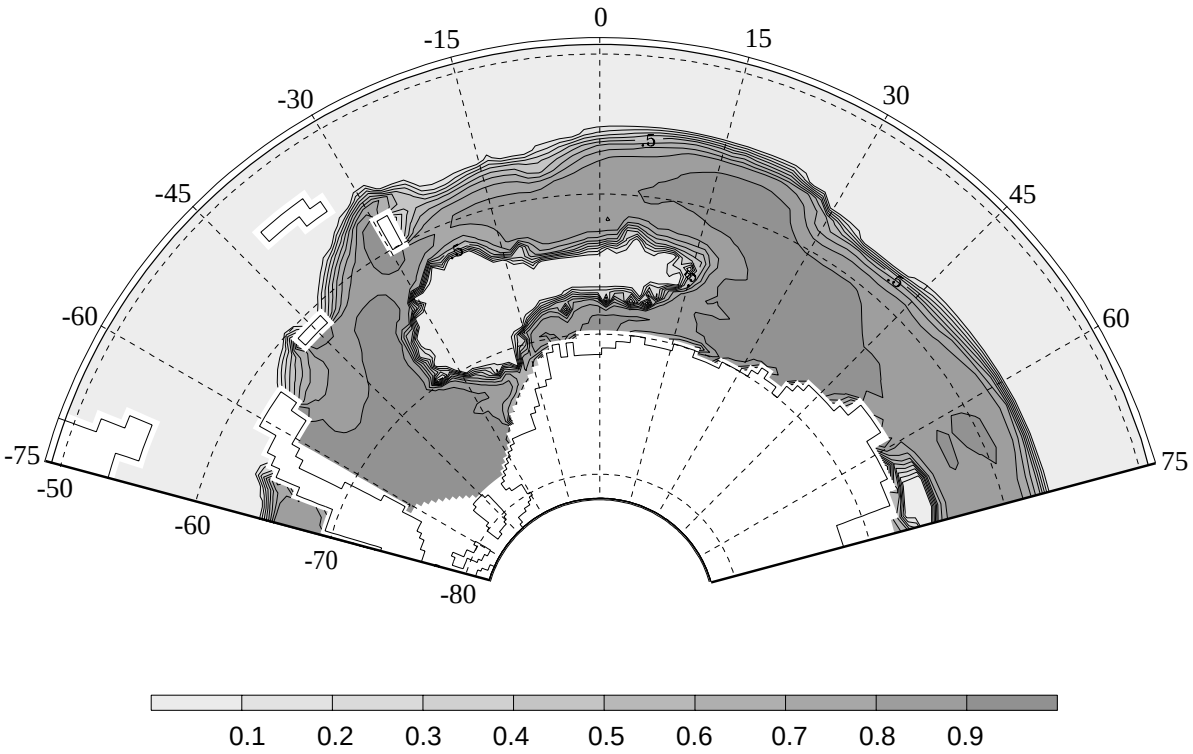

Figure 10. Monthly mean (September 1993) simulated sea ice concentrations in the Weddell Sea sector using a convective adjustment scheme to treat static instability.

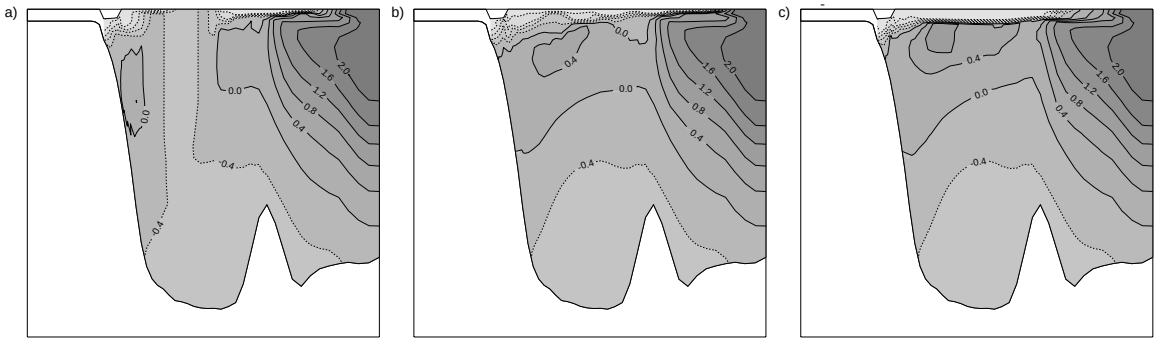

Figure 11. Meridional section of potential temperature along 18°W from experiments with different parameterizations of convection. Displayed are simulated monthly means from September of the ninth year of integration using a) convective adjustment, b) a vertical diffusivity of 0.01 $m^2\ s^{-1}$ in case of static instability and c) the *Pacanowski and Philander* [1986] mixing scheme with vertical diffusivity limited to values below 0.01 $m^2\ s^{-1}$.